Source inversion of regional intensity patterns of five earthquakes from south-western Norway

F. Pettenati[1], L. Sirovich[1], H. Bungum[2] and J. Schweitzer[2]

[1] *Istituto Nazionale di Oceanografia e di Geofisica Sperimentale - OGS, Trieste, Italy*

[2] *NORSAR, Kjeller, Norway*

(Received January 18, 2005; accepted April 27, 2005)

ABSTRACT An intensity-based source-inversion technique, that earlier was applied only to larger earthquakes, has been tested on the basis of regional macroseismic intensity patterns from four recent earthquakes in south-western Norway for which high-quality instrumental data have provided independent assessments of magnitudes, locations and fault-plane solutions. In spite of the modest magnitudes of the earthquakes (M_L 4.0-5.2) and the asymmetry of the sampled area due to the proximity to the coast, the test was satisfactory enough in that the inversion results for three out of the four events studied came close to the independent solutions from instrumental data. In addition, we inverted the intensity data from a 1954, M_L 4.5, earthquake from the same region for which independent instrumental data are lacking, and found results that are consistent with our present understanding of the seismotectonics in this region. The method is based on the inversion of a kinematic function that represents the ground motion, at a given point on the surface, from a line source. Since the problem is non-linear and possibly also bimodal, we used a sharing Niching Genetic Algorithm to perform the inversion. The inversion includes a number of source parametres, the most sensitive of which were the hypocentral coordinates and the fault-plane parametres. The parametres obtained for the south-western Norway earthquakes studied here were generally stable except for the epicentral longitude, due to the partial lack of data towards the offshore (North Sea) region to the west. The present study has shown that it is possible to extend this type of inversion of earthquake intensity data to lower magnitudes, sometimes even in cases when the sampling from the felt area is asymmetric. As such, the results achieved encourage the use of this method also for historical, pre-instrumental earthquakes also from low-seismicity regions. This opens the way for significant advances based on historical data that earlier could be used only for a broader assessment of earthquake locations and magnitudes.

1. Introduction

In seismically active regions at plate margins, the return period for the largest earthquakes is of the order of 100 years, while for regions in the interior of plates the return period may be thousands of years (e.g., Bungum *et al.*, 2004). When considering the fact that good instrumental data have been available, at best, only for the last 50 years, it becomes of utmost importance to be able to extract as much information as possible from older macroseismic intensity data. Such data have, in many parts of the world, been systematically collected and analyzed already from the last part of the 19th century, when seismology started to become a science. Felt information

from earthquakes are available in a less systematic form, for hundreds, and in some cases even thousands of years (e.g., Italy, Greece, Middle East, China). Up to recently, macroseismic data could be used, albeit with significant uncertainties, essentially only for assessing epicentral locations inferred from intensity distribution, and for determining magnitudes or equivalent seismic moments either from maximum intensity (e.g., Camassi and Stucchi, 1997) or from the areas covered by different intensity levels (e.g., Muir Wood *et al.*, 1988; Johnston, 1996). Valuable results have recently been obtained, however, after intensity (I) was analysed with new, more quantitative techniques (e.g. Frankel, 1994; Johnston, 1996a, 1996b; Bakun and Wentworth, 1997). We would also like to note here the pioneering attempt by Shebalin (1973) to use the highest isoseismal for determining the shallowest depth of the rupture, and the remaining isoseismals for estimating its average depth. All of these efforts have rendered macroseismic data important also for the evaluation of seismic hazard and risk.

This recognition of the information potentials in available intensity data has been the basic motivation behind an effort by some of the present authors over the last few years (Sirovich, 1997; Pettenati *et al.*, 1999; Sirovich and Pettenati, 2001, 2004; Sirovich *et al.*, 2001, 2002; Pettenati and Sirovich, 2003; Gentile *et al.*, 2004) to develop a more systematic approach for inversion of macroseismic data, and to validate the results through comparisons with independently recorded instrumental data. Based on either a Niching Genetic Algorithm (NGA) or a grid-search approach, the intensity field is inverted for the following parametres: the nucleation point (latitude, longitude and depth), the focal mechanism (strike, dip and rake angles), the seismic moment M_0, the S-wave velocity in the half-space Vs, and the along-strike and antistrike Mach number Vr/Vs, where Vr is the rupture velocity. In this study, the 11th unknown inversion parametre is the percentage of the along-strike rupture length over the total rupture length, L_{tot}. Note that the total length of the rupture (i.e., the source dimension) L_{tot} is the sum of the along-strike part and the antistrike dimensions, and that we derive the total length of the source from the seismic moment M_0 via the Hanks and Kanamori (1979) empirical relation

$$M_W = 2/3(\log M_0) - 6.06 \quad (1)$$

and the Wells and Coppersmith (1994) relation

$$\log L_{tot} = -2.44 + 0.59 M_W, \quad (2)$$

where M_W is the moment magnitude.

Genetic algorithms (GAs) are used here in a rough analogy with biology in the sense that each of our sources is treated as an individual with 11 genes (i.e., 11 source parametres). For a simplified introduction to the NGA global optimization technique, see Martin *et al.* (1992). In general, GAs have already been applied to a suite of seismological problems (e.g., Kennett and Sambridge, 1992; Koper *et al.*, 1999; Moya *et al.*, 2000).

Recently, this source inversion technique was validated by comparing results based on regional macroseismic intensity patterns with those obtained from instrumental data, for the 1987 5.9 magnitude Whittier Narrows earthquake in southern California (Pettenati and Sirovich, 2003; Gentile *et al.*, 2004). Similar studies have also been conducted for the 1994 Northridge (Pettenati *et al.*, 1999) and for the 1991 Sierra Madre earthquakes (Sirovich *et al.*, 2001). Under less favourable conditions the technique was also tested for a 1936 earthquake in north-east Italy

(Sirovich and Pettenati, 2004), and for an earthquake in Sicily in 1990 (Sirovich and Pettenati, 1999), as well as for two strong destructive events from the 17th century in Sicily (Sirovich and Pettenati, 1999, 2001). In the first case, the grid-search inversion was validated by a close constraint around the instrumental hypocentral coordinates, while in the latter case the inversion produced source models that are fully compatible with the seismotectonics and with the stress conditions in that area (Sirovich and Pettenati, 1999, 2001).

In the present paper, an effort is made to extend the method to lower magnitudes and to more stable continental regions by inverting macroseismic observations from five medium-to-low local magnitude (M_L 4.0-5.2) earthquakes that have occurred along the western coast of Norway during the last 50 years. A detailed comparison with results from instrumental measurements has been possible in all but the oldest one of these events, thereby offering independently established locations, magnitudes and focal mechanism solutions. Besides low magnitudes, these events are posing an additional challenge in that they are located in a coastal region, with asymmetric sampling of the intensity field.

2. Intensity inversion methodology

Since the methodology applied in the present paper was well documented earlier [Sirovich (1996, 1997) for the *KF* model, Sirovich and Pettenati (2001, 2004) and Pettenati and Sirovich (2003) for the inversion method], we will only provide a brief description. The methodology is based on expressing the radiation from an earthquake in terms of the dimensionless values of a kinematic function *KF* which is the contribution of a source point (the rupture propagating along a linear fault at depth *H*), at a distance *l* from the nucleation point, to the displacement-related ground motion at the receiver point *P* on the surface:

$$KF(P,l) = \frac{R(P,l)}{D(P,l)[1-(Vr/Vs)\cos\theta(P,l)]} \quad , \tag{3}$$

where *R* is the radiation pattern of S-waves (Aki and Richards, 1980), $D(P,l)$ is the distance between source-receiver points, *Vr* is the rupture velocity, *Vs* is the S-wave velocity, and θ is the angle between the ray reaching *P* and the direction of the rupture propagation. As already noted there are eleven parametres to invert.

The *KF* model rests upon an asymptotic assumption which is satisfactory at distances from the source as close as the order of the wavelength (Bernard and Madariaga, 1984; Spudich and Frazer, 1984; Madariaga and Bernard, 1985), while beyond 80-100 km the amplitudes of surface waves progressively prevail over those of body-waves. According to this, during the present inversions, all sites closer than 5 km to the projection of each tentative line source received the maximum *KF* value calculated at the site closest to the source, but outside the 5 km limit.

We are aware that our methodology is, as often is the case in science, a compromise between model complexity and the quality of the empirical data. This means, in particular, that we could not introduce more parametres for the crustal model for more wave types; moreover the asymptotic assumption results in a limitation of the range of distances and frequencies within which it might be reasonable to operate [see the rule of thumb by Spudich and Frazer (1984)].

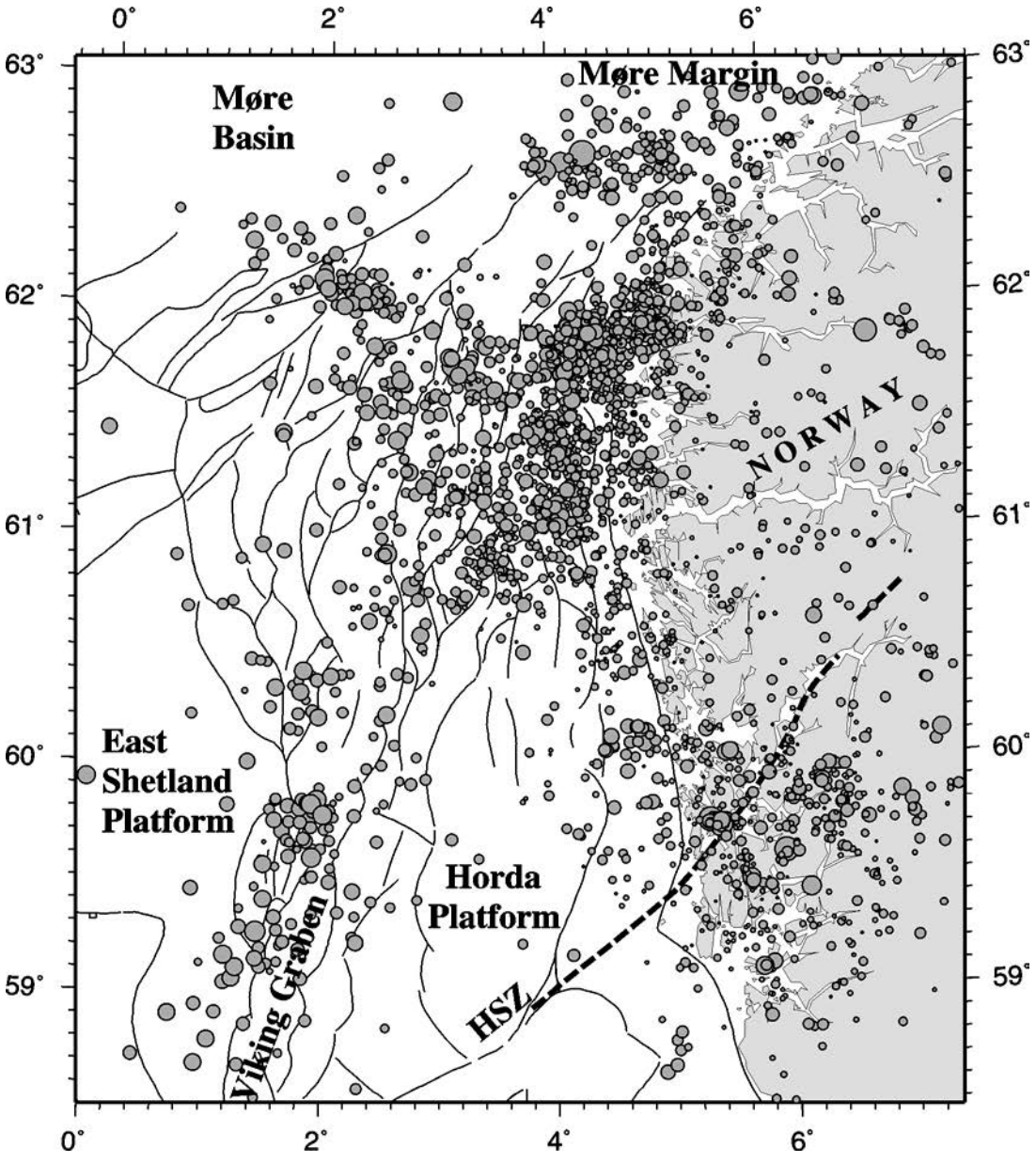

Fig. 1 - Earthquakes in the western Norway region for the time period between 1984 and 2004 (University of Bergen, 2004). The thin black lines are mapped faults and the heavily dashed black line HSZ is the Hardangerfjorden Shear Zone [redrawn from Møllegaard (2000)].

For the definition of the Cartesian coordinates used we refer to Fig. 1 of Sirovich (1997) or to Fig. 1 of Pettenati and Sirovich (2003). The positive direction of the strike is ranging from 0º to 360º, with the plane dipping to the right, while the rake angle is seen on the fault plane from the hanging wall and measured counter-clockwise between the positive direction of the strike and the direction of the slip vector. In this way, rake angles ranging between 1º and 179º indicate faults

with inverse (compressive) components. The total length of the rupture L_{tot} is the sum of the absolute values of the along-strike length and the antistrike one. The along-strike part is considered positive ($L+$); the antistrike one is negative ($L-$); the same holds for the Mach numbers ($Mach+$ and $Mach-$).

The *KF* procedure is unable to discriminate between the results produced by mechanisms that differ by 180° in the rake angle, because in both cases it produces the same radiation but with reversed polarities. This ambiguity, which comes in addition to the classical focal mechanism solution ambiguity between fault and auxiliary plane, may be solved only with additional geological information. Thus, the black and white shadings of the fault-plane solutions obtained from our inversions in the following figures could be reversed; we show distensive or compressive mechanisms according to the fault-plane solutions obtained from instrumental measurements.

Given the definition of *KF* in Eq. (3), we then calculate pseudo-intensities *i* at location (x,y) by the linear multiple regression [Eq. (4)], which was obtained by treating 1720 site intensities observed by the US Geological Survey after five earthquakes in the greater Los Angeles region (Sirovich and Pettenati, 1999):

$$i(x,y) = 9.241\,(\pm 0.152) + 3.358\,(\pm 0.124)\cdot m[\log_{10} KF(x,y)] + [8.04\,(\pm 0.54)\cdot 10^{-20}]\cdot M_0 \qquad (4)$$

where $m[\log_{10} KF(x,y)]$ represents the median values of $\log_{10} KF(x,y)$ per intensity class, with $KF(x,y)$ being the maximum (non-dimensional) value calculated at location (x,y) by Eq. (3), while M_0 is the seismic moment (in N·m). The standard errors of the coefficients are also indicated in Eq. (4). While in this paper *I* expresses the macroseismic intensity as referred to its proper scale, *i* is a pseudo-intensity which expresses the macroseismic intensity treated as a real, or integer, number. We stress that Eq. (4) should ideally be used only within the calibration ranges of the aforementioned 1720 empirical data points, namely $2.7\cdot 10^{17} \le M_0 \le 2.2\cdot 10^{19}$ N·m (corresponding to $5.5 \le M_W \le 6.8$), IV≤*I*≤IX, and $-3.260 \le \log KF \le -0.108$ (Sirovich and Pettenati, 1999). Since the magnitudes and intensities used in this study are, for the greater part, below this range and therefore need to be extrapolated, this introduces an additional level of uncertainty. Even so, we claim that this extrapolation, needed here since sufficient data to calculate a new regional specific correlation were not available for the Norwegian earthquakes, has a limited influence on the shape of the radiated synthetic fields**.** This is supported by the fact that the analysis of five Californian earthquakes has shown, within the range given above, that the correlations *i/logKF* translate rigidly downwards in the seismic moment [see Fig. 1 in Sirovich *et al.* (2001)].

Since the inversion of the *KF* function is a non-linear problem in this case, we used a NGA with the sharing mode already experimented successfully in the above-mentioned cases. In terms of global optimization and computational costs, GAs provide advantages over other randomized search schemes (e.g. local optimization), which easily could, moreover, be biased by the starting conditions. The total number of function evaluations in NGA is much smaller than in a grid-search because the models of a new generation are selected so as to exploit the good information of the parent generation and, in general, in order to have a better fitness as well. It is self-evident that the present inversion technique performs closest to optimal when the intensity field is well

sampled, and when local amplification effects are not affecting groups of neighbouring sites. These conditions were particularly well met for the 1987 Whittier Narrows and for the 1936 Bosco Cansiglio earthquakes (Gentile *et al.*, 2004; Sirovich and Pettenati, 2004), where the intensities were based on the MMI and MCS scales, respectively.

On the other hand, cases when the sampling has been less uniform due to the proximity of coastal areas, were also covered earlier (Sirovich and Pettenati, 1999, 2001). This is the situation we are faced with in the present study.

2.1. The inversion procedure

The NGA used in this study is based on routines from the Parallel Genetic Algorithm Library by Levine (1996). We used, and explained, the same technique more thoroughly in two recent papers (Gentile *et al.*, 2004; Sirovich and Pettenati, 2004). In short, while the grid-search technique calculates all possible solutions with a highly time-consuming process, the GA approach is based on a sampling of the most favourable sub-hyperspaces of the source parametres of the model. To this end the NGA is, in particular, performing the GA tasks, but mostly with respect to problems that have more than one solution, since they introduce the niching conditions.

For our grid-search, GA, and NGA applications we adopted the same fitness criterion (objective function): the sum of the squared residuals, Σr_s^2, where r_s is the pseudo-intensity i calculated at each site by Eqs. (3) and (4), minus the intensity I observed at the same site, where the subscript denotes the sites. The main steps of NGA are: 1) the *selection* process, which chooses the individuals by evaluating their fitness criterion (Σr_s^2), and produces a new intermediate generation with the best fit (elitistic selection); 2) the *crossover*, which randomly chooses the parental models with 90% fertility; 3) the *mutation*, which randomly changes one of the source parametres, of 6% of the sources of the new generation; 4) the *crowding*, which deletes identical individuals, and prevents the population from quickly converging to a false minimum; and 5) the *sharing*, which works by making the demes (subpopulations) explore the whole of the residuals' hyperspace. Points 1-5 allow different subpopulations of sources to survive within parametric sub-spaces (niches), so that each source of one subpopulation is not in competition with the individuals of other demes living in other niches.

We used four demes (subpopulations) each of 2,000 individuals (i.e. sources), each deme evolving independently because, in the aforementioned *sharing* step, the normalized distance *Dd* between each individual of a deme and each individual of all the other demes obeys the following condition:

$$Dd(\mathrm{x},\mathrm{y}) = \frac{1}{n}\sum_{i=1}^{n}\frac{|x_i - y_i|}{b_i - a_i} \qquad (5)$$

where n is the number of the unknown parametres (11, in our case); x_i = ith parameter of an individual from deme x; y_i = ith parameter of an individual from deme y; b_i = the upper bound of the ith parameter; and a_i = the lower bound of the ith parameter. Thus, *Dd* is the mutual, normalized, distance between source models (individuals) in the 11-dimension hyperspace of the source parametres, in fact, *Dd* varies from 0, for identical models, to 1 for two models at opposite ends of the search boundary (Koper *et al.*, 1999). The distance *Dd* has to be tuned for each study case by trial and error because, if the distance is too high, some demes will not reach any solution;

if the distance is too low, all demes will converge toward the same depression of the hypersurface of the residuals, but often without the ability to catch the best source solution. The way in which errors of each single parameter are calculated is described by Pettenati and Sirovich (2003) and Gentile *et al.* (2004), where the complete inversion method is described in more detail. The errors in this study are calculated with the bootstrap method, and estimated with two standard deviations. The bootstrap is an internationally recognized technique for artificial data randomization when you don't know enough about the underlying process, or the nature of your measurement errors (Press *et al.*1992).

3. Data analysis

The present study is concerned with a number of smaller earthquakes in the coastal region of south-western Norway, to be described and discussed in more detail below, following a brief introduction to the seismotectonic conditions in the region.

3.1. Seismotectonics of western Norway

Western Norway is one of the most seismically active regions in north-western Europe (Bungum *et al.*, 1991), with a number of earthquakes above magnitude 5 occurring during historical times (Muir Wood *et al.*, 1988; Hansen *et al.*, 1989). The region shown in Fig. 1 is a transition zone between three different seismotectonic regimes. To the north, the seismicity is affected by the mid-Norwegian Møre continental Margin (see Fig. 1), including areas with thick Plio-Pleistocene deposition centres (Byrkjeland *et al.*, 2000). To the SW, the seismicity extends into the Viking Graben, with crustal thinning and extensional deformation (Havskov and Bungum, 1987), while to the southeast the seismicity follows the coast, usually with shallower seismicity and quite diverse faulting patterns (Hicks and Ottemöller, 2001). For all of these offshore regions earthquake focal mechanisms as well as in situ measurements reflect, to a first order, a dominating NW-SE compressive stress, consistent with the ridge push force (Hicks *et al.*, 2000a). Even so, the crustal stress field also reflects clear influences from regional and local sources of stress (Byrkjeland *et al.*, 2000; Hicks *et al.*, 2000b; Bungum *et al.*, 2004).

For the region in between these three areas with different seismotectonic regimes in the North Sea, around 61°N to 62°N latitude, the seismicity is transitional and quite complex, as reflected, in particular, in the fact that the maximum horizontal stress as inferred from some of the events exhibits a 90º rotation of the P and T axes (Hicks *et al.*, 2000a). South of this region, between the Viking Graben and the coast, the Horda Platform is almost entirely without seismicity (Fig. 1). All the earthquakes in all of these regions seem to occur in the crystalline basement, also offshore where thick sedimentary deposits may be present.

The south-eastern coastal region shown in Fig. 1, including the Stord-Bømlo area as shown in more detail in Fig. 2, is part of the Caledonian mountain range. The region is crossed by the NE-SW trending Hardangerfjorden Shear Zone which separates the Precambrian basement rocks to the southeast from the Caledonian rocks to the NW, crossed by a series of N-S and NNW-SSE trending faults (see the subsequent Fig. 9). This is the setting for the earthquakes analyzed in this study.

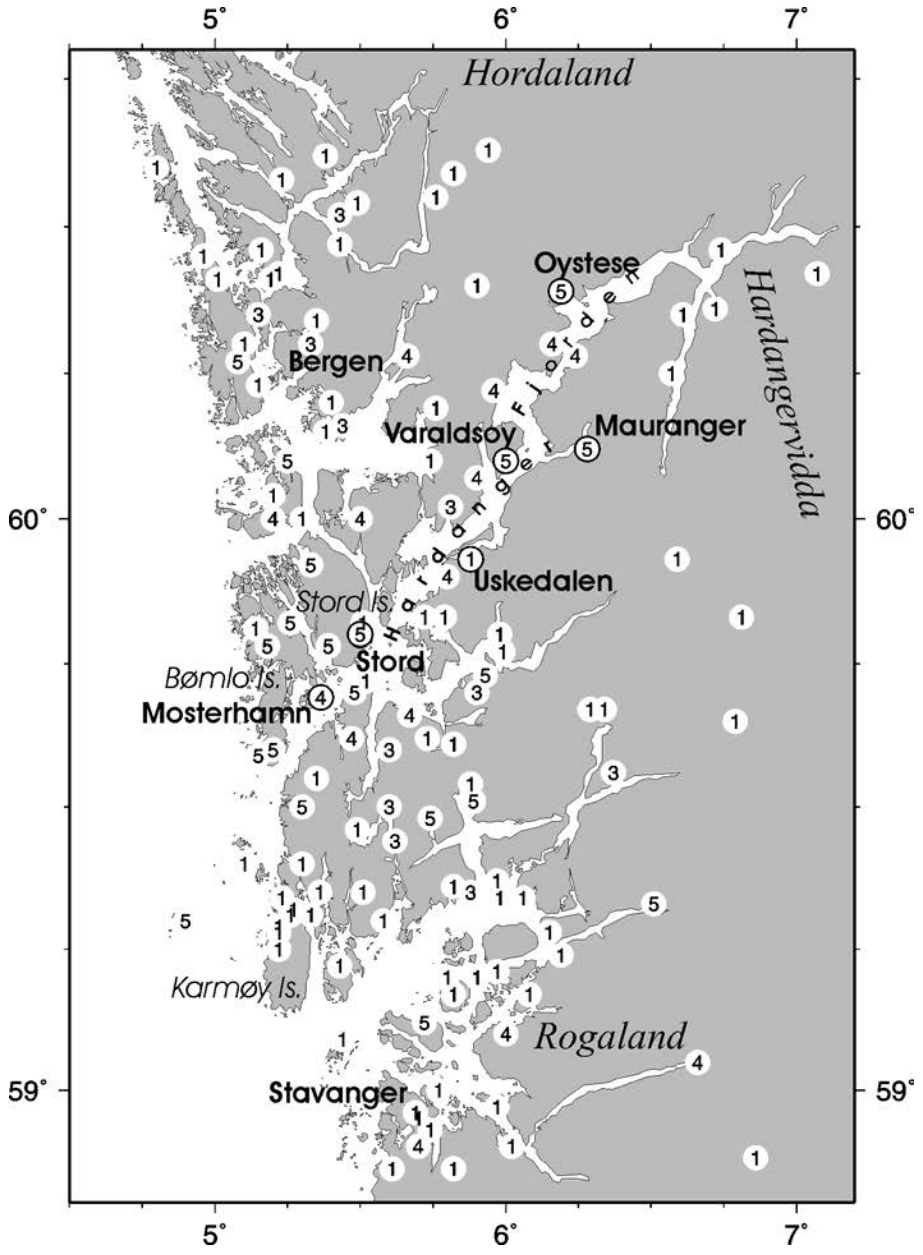

Fig. 2 - E2 earthquake of Dec. 8, 2000 (see Table 1). Intensities observed at the sites, "not felt" data included [i.e., intensities "1"; University of Bergen (2003)]. The encircled values refer to the sites of Fig. 3.

3.2. Earthquakes studied

The main part of the present study is concerned with validation tests where we have selected four earthquakes E1 to E4 as listed in Table 1, where also earlier-determined hypocentre and focal mechanism solutions as obtained from instrumental data are provided. These events occurred between 1983 and 2000 (note that they are not listed chronologically), with magnitudes between 4.0 and 5.2. The first two of the earthquakes (E1 and E2) are located south of Bergen in the Stord

Table 1 - The available intensity data, and the reference parameters obtained from instrumental measurements, which are used for the present validation. The angular values of the theoretical auxiliary planes of the solutions shown are added in round parentheses. Event E1 is from the Stord-Bømlo area (Havskov and Bungum, 1987), E2 is also from the Stord-Bømlo area (Hicks and Ottemöller, 2001), E3 is from the south of Bergen (University of Bergen, 2004), and E4 is from the North Sea (Hansen *et al.*, 1989).

Event Parameters	**E1 (93 data) 03.08.1983 18:43, M_L 4.4**	**E2 (41 data) 08.12.2000 14:27, M_L 4.5**	**E3 (69 data) 01.29.1989 16:38, M_L 4.0**	**E4 (75 data) 01.23.1989 14:06, M_w 5.2**
Lat. N [°]	59.70 [59.66]*	59.76	59.77	61.97
Long. E [°]	5.40 [5.23]*	5.34	6.00	4.43
strike [°]	35 (145.0)*	333 (192.2)	136 (255.0)	20 (232.4)
rake [°]	150 (42.3)*	58 (114.0)	305 (216.5)	70 (116.0)
dip [°]	52 (66.5)*	40 (57.0)	67 (41.0)	55 (39.7)
depth [km]	15	18	7	24-28
M_0 [Nm]·10^{15}	6.99	9.54	2.1	60.0

* according to the catalogue of the University of Bergen (2004), the rupture plane corresponds to the auxiliary plane of the solution by Havskov and Bungum (1987); the epicentral coordinates by the University of Bergen (2004) are in square brackets.

and Bømlo Islands area, the third one (E3) is located further inland at about the same latitude, while the last one (E4) is located offshore in the northern part of the North Sea (see the subsequent Fig. 5). A summarized description of these events can be found in Bungum *et al.* (1991).

The selection of these earthquakes was determined exclusively on the basis of what was available in terms of magnitude coverage, instrumental solutions, and intensity data. At least 41 site intensities are available for each of these events, and all of them cover at least three intensity degrees. In this way, these events include the most significant earthquakes in this region since the beginning of the 1980s, when the local seismological network in this region was deployed by the University of Bergen. In Table 1, the geometrical parametres of the principal planes are shown first, followed by those of their auxiliaries in the fault plane solutions. Note, however, that in the case of the event E1, the earthquake catalogue of the University of Bergen (2004) gives credit to a slightly different epicentre, and to a rupture plane which corresponds to the auxiliary plane of the principal solution developed by Havskov and Bungum (1987).

All of the macroseismic data used are from the University of Bergen (2003) catalogue and are expressed in the EMS98 scale. Some of the intensities in this catalogue are reported with intermediate values, for example 4.5 for values in the range IV-V, and in these cases we have, as an a priori choice, used the upper value (V in this case). Given the distance limit where the body waves approximately prevail [see our comments to Eq. (3)], we used only the macroseismic data limited to an area within 200×200 km, centred at the instrumental epicentre. We thus obtained data in the range $I \leq I \leq$ VI. We also decided to eliminate all of the $I = 1$ values, since the "not felt" reports are given a value of 1 in the EMS98 scale. In the data sets from the E1, E3 and E4 events there are only very few sites with an I=1 degree (however, never more than three). On the other hand, for event E2 of 2000 there were 83 "not felt" reports out of a total of 125 (67%) because in recent times the University of Bergen (2003) extended the investigated area.

Fig. 2 shows the complex situation for the original macroseismic data set for event E2; note, in particular, the many "not felt" (=1) reports, occurring also in the epicentral area, where at the

same time several degrees IV and V were reported. A possible explanation for this could be that this earthquake occurred just after noon in mid summer, with many witnesses finding themselves on the road, therefore not feeling the earthquake. Event E4, by comparison, occurred at approximately the same time, but in January, with most people indoors. An important perspective here is that all of the data are below the VI degree, and that even at the V degree level the definition is that "the earthquake is felt indoors by most, outdoors by few…". Finally, E1, E3 and E4 occurred in the 1980s, whilst E2 happened in 2000; thus, the criterion for storing the "not felt" reports could have changed in the meantime.

3.3. Site effects and outliers

It is worth noting at this stage that several anomalous seismic responses concentrated in sub-regions could bias source inversion results [e.g. see the concentration of damage along the southern slope of the Puente Hills, due to local normalized amplification during the Whittier Narrows, 1987 earthquake (Kawase and Aki, 1990)]. On the other hand, single and sparse anomalous sites would simply increase the inversion noise. With this in mind, we looked for site effects first. Unfortunately, no systematic geological or geomorphological information was available for all sites, even though it is known that deeper soft soil deposits are very rare in this region where hard rocks generally prevail. Thus, we started our analyses by building the seismic site histories according to Azzaro *et al.* (1999). In particular, we examined all of the sites that could possibly contain anomalous intensity values, starting with the sites that contained reported intensities from a sufficiently large number of events. To this end, we examined the entire University of Bergen catalogue covering the period 1976-2001.

The results for six sites are given in Fig. 3, where Fig. 3a shows the seismic site history of the Mosterhamn site (which is one of the more 'suspected' ones, as discussed below; see Table 2 also). The poles with the square on the top indicate the epicentral values (*Io*), while the circles are the intensity at the site for the same event. A normal behaviour here, unbiased by site effects, would be that outside the epicentral area the distance between the squares and the circles would increase with distance, reflecting the intensity attenuation. Fig. 3a could suggest some amplification in two cases at approximately 30 km epicentral distances (also see later that intensity IV at something less than 30 km is a statistical outlier); but no evidence of systematic and significant local effects is found.

In all the other five cases, in Fig. 3, the situation is more heterogeneous. For the Stord site Fig. 3b, there is an intensity $I = 4\text{-}5(=Io)$ at a 44 km distance (which is a statistical outlier; see

Table 2 - List of outliers in the data sets of the E1-E4 earthquakes studied.

Event	Site	Lat. [°]	Long. [°]	*I*
E2	Mosterhamn	59.70 N	5.40 E	IV
E3	Mosterhamn	59.70 N	5.40 E	III
E3	South of Litlabø	59.77 N	5.39 E	III
E3	Stord	59.80 N	5.49 E	IV-V
E3	Sauda	59.67 N	5.33 E	IV-V
E3	Litlabø	59.80 N	5.40 E	V
E4	Vaagsvaag	61.95 N	5.05 E	IV
E4	Instevik	61.10 N	6.01 E	IV

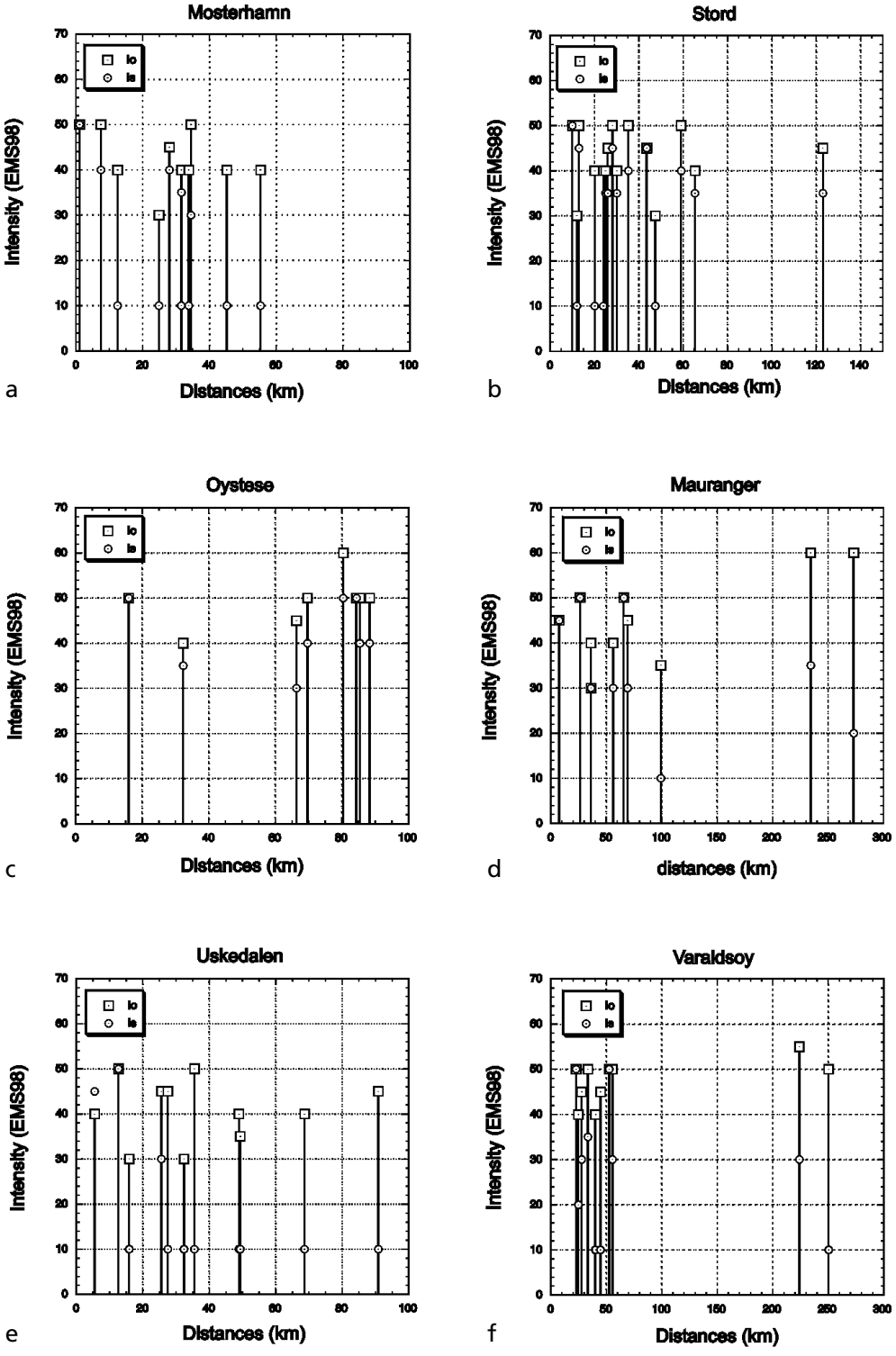

Fig. 3 - A sample of the seismic histories observed at six sites (intensity versus epicentral distance; intensities are from the catalogue by the University of Bergen, 2003). See the locations of the sites in Fig. 2. Note the factor of ten in the EMS98 intensity scale.

later, and Table 2), possibly indicating a site amplification at that distance. However, in various cases, and at a range of distances, the site intensities at Stord are rather low with respect to *Io*, indicating that there is no systematic amplification which could significantly bias the inversion. The remaining sites in Fig. 3c to 3f are from the Hardangerfjorden area (for locations see Fig. 2), NE of the E1 and E2 epicentres. The reason for this choice is that for these two earthquakes some intensity data higher than expected are found in this direction, which, in theory, could be due to either source, path or site effects. Fig. 3c to 3f suggest that site effects cannot be evoked in this case, which is the case also for other sites that have been checked, but are not shown here. In fact, out of all the sites located NE of the E1 and E2 epicentres, only Oystese (Fig. 3c) has consistently high intensities, Mauranger (Fig. 3d) shows some symptoms of amplification at distances shorter than 70 km, whereas the others, Uskedalen (Fig. 3e) and Varaldsoy (Fig. 3f), reveal an inconsistent behaviour.

We stress, however, that the limited influence of the site characteristics on regional intensity patterns in this area does not necessarily contradict other factors related to local amplifications of macroseismic intensity. A case like that was discussed by Sirovich (1982) who experienced amplifications and de-amplifications of one to two *I* units within towns and hamlets struck by an earthquake in southern Italy. Since the catalogue used here reports only one intensity datum per site, the effect of a microzone could easily be swamped by those of the other microzones, that contribute to the classification of each *I* degree for each town. It has been noted by Shebalin (2003), in this respect, that "the intensity is relevant for an area [and] has a statistical nature, so it is more stable than single-site peak ground acceleration measurements" (Molchan *et al.*, 2004).

We also looked at the matter of site effects from a statistical point of view by searching for outliers in the intensity/distance data set for each earthquake, given that outliers could mean anomalous seismic responses, but possibly also survey or transcription errors. Thus, given the log-normal statistical model, we analyzed the distribution of the logarithms of the epicentral distances *d(I)* for each earthquake with the classical Chauvenet method (Barnett and Lewis, 1978; Johnston, 1996). Using this technique, in an analysis of the data sets of the four earthquakes studied, we found the intensity outliers *I* shown in the 5th column of Table 2. The Mosterhamn site, which already attracted our attention, is the only one to have been identified as an outlier in two earthquakes E2 (at 7 km distance) and E3 (at 34 km). In both cases, the *I* values at this site, which is located at the southern end of Stord Island (see Fig. 2), are too low. The other sites appear in Table 2 only once, therefore their effects, if any, would not be systematic.

The conclusion from this search for site effects and outliers is that it seems that one can exclude evident effects that systematically could bias our source inversions.

4. Results of intensity inversions

4.1. Exploration of the residuals' hyperspace

In the present inversions we employed the NGA in the exploration of the whole hyperspace of the intensity residuals r_s with no constraints on the angular parametres of the fault-plane solution; thus, the strike went from 0° to 359°, and the rake angle from 0° to 179°, in both cases with a 1° step length. We omitted dip angles below 20° because they are unrealistic, thereby exploring the range 20°-90°, again with a 1° step length. The rest of the parametres were allowed to vary within reasonable ranges. In particular, given the coordinates of the instrumental epicentre, the latitude

range explored by the NGA was ±0.25° (±28 km), and the longitude range was ±0.45° (±50 km). The exploration range for M_0 was from $1 \cdot 10^{15}$ to $9.9 \cdot 10^{15}$ N·m (corresponding to M_w 3.9-4.6) for events E1, E2, and E3, and from $5 \cdot 10^{15}$ to $9 \cdot 10^{16}$ N·m (M_w 4.4-5.2) for event E4. Besides this, we adopt a more severe constraint only for *Vs* (*Vs* = 3.60+/-0.05 km/s), because we trusted the crustal model by Havskov and Bungum (1987), which is often used to calculate the focal mechanisms in this area.

To make the demes (model sub-populations) explore the whole hyperspace of the intensity residuals r_s we had to tune the distance for each earthquake as defined in Eq. (5). This is a critical step of the inversion because the hyperspace of the residuals is highly irregular (see for example the irregular topography in Fig. 4). Table 3 presents the minimum-variance models found by the NGA inversions, and Fig. 4 shows an example of the exploration of the topography of the squared pseudo-intensity residuals Σr_s^2 at the surveyed sites in the hyperspace of the parametres of the fault-plane solution of earthquake E4. In this figure, Σr_s^2 varies from more than 250 (black) to less than 25 (white). The minimum variance solution obtained for E4, with Σr_s^2 = 20, is marked by an open cross, in the box corresponding to the 68° dip angle (see also Table 1).

In Fig. 5, we present a direct comparison between the epicentres and the fault-plane solutions already available from instrumental measurements, and those determined in the present study (remember the 180° ambiguity in the rake angle). We stress that the figure shows the most recent epicentre of event E1, that is the one from the new earthquake catalogue of the University of Bergen (2004).

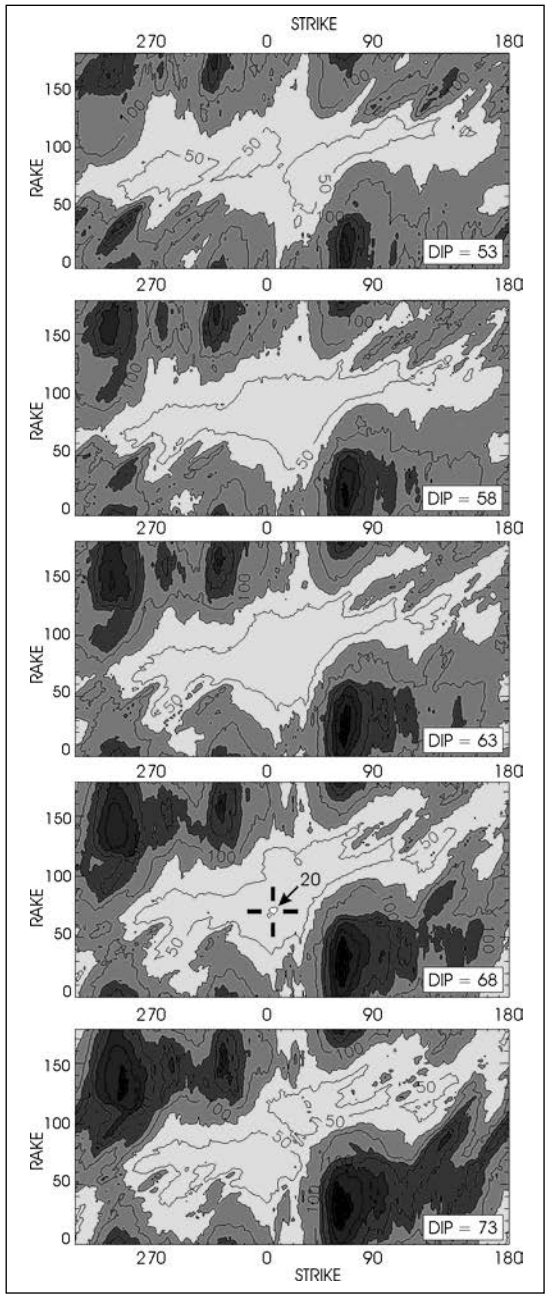

Fig. 4 - The topography of the squared pseudo-intensity residuals Σr_s^2 at the surveyed sites in the hyperspace of the parameters of the fault-plane solution of earthquake E4 (see Tables 1 and 3).

4.2. Validation results

The basic validation test in the present case is concerned with to which extent the source inversion results, based on the regional intensity data, match results obtained from other and independent studies, based on instrumental data.

Table 3 - Source parameters obtained from the inversions of macroseismic data; errors were calculated with two standard deviations. Auxiliary solutions are in parentheses.

Earthquake/Parameters	**E1** **03.08.1983**	**E2** **08.12.2000**	**E3** **01.29.1989**	**E4** **01.23.1989**
Lat. [°] N	59.74±0.04	59.74±0.07	59.81±0.06	61.97±0.07
Long. [°] E	5.02±0.08	5.17±0.04	6.20±0.11	4.65±0.12
strike [°]	344±5 (214.2)	320±12 (230.0)	156±10 (7.0)	4±9 (223.0)
rake [°] (±180°)	59±8 (131.7)	39±10 (178.7)	260±14 (300.0)	73±7 (125.9)
dip [°]	60±5 (42.0)	90±7 (51.0)	73±6 (19.6)	68±4 (27.5)
M_0 [Nm]$\cdot 10^{15}$	4±0.4	6±2	4±1.6	60±4.2
Mach +	0.77±0.05	0.66±0.08	0.60±0.05	0.92±0.07
Mach -	0.74±0.04	0.63±0.04	0.60±0.04	0.92±0.05
Vs [km/sec]	3.60±0.07	3.65±0.06	3.54±0.06	3.65+0.09
Ltot [km] L+ = / L- =	1.35 0.10 / 1.25	1.58 0.78 / 0.80	1.35 0.05 / 1.30	3.90 3.82 / 0.08
$\sum r_s^2$	74	17	36	20

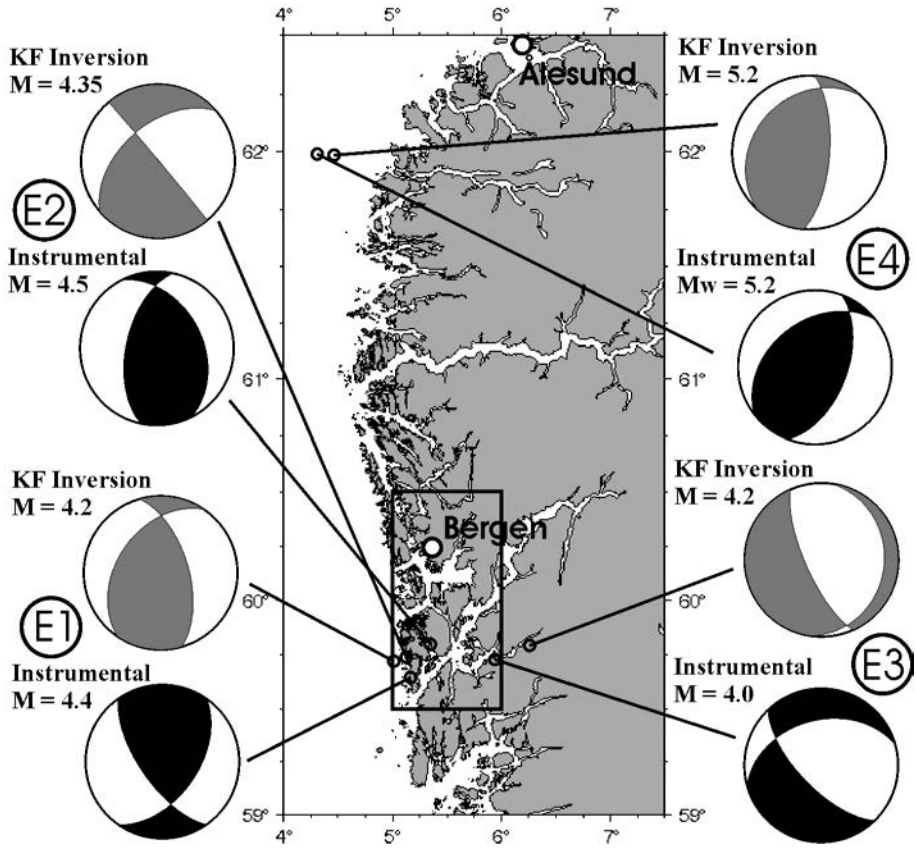

Fig. 5 - Direct comparison between the epicentres and the fault-plane solutions already available from instrumental measurements, and those determined in the present study (there is an intrinsic ±180° ambiguity in the rake angles obtained from our inversions; see the text).

For event E1 (Fig. 5, lower left), the inverted and the instrumental epicentres are not far from each other; however, the present strike and rake angles do not match the reference values obtained by Havskov and Bungum (1987) well (see Table 1). Even so, the dip angle is compatible, the overall retrieved mechanism is not very different, and, even more important, the inferred E-W direction of maximum compressive stress is quite similar and consistent with what is generally observed in this region (Bungum *et al.*, 1991; Hicks *et al.*, 2000a). It is worth noting that also the second-quality minimum-variance solution obtained in the present inversion for event E1 has strike, dip and rake quite compatible with the reference solution by Havskov and Bungum (1987) in Table 1. It could also be noted that event E1 occurred just after the installation of the local network operated by the University of Bergen, and that Havskov and Bungum (1987) and the University of Bergen (2004) are in disagreement on the question of which of the two planes is the real rupture plane. We still conclude that the test was positive in this case.

For event E2 (Fig. 5, upper left), we find that the NGA inversion has, also in this case, caught the epicentral latitude as well as the strike and rake angles of the principal plane satisfactorily [as compared to Hicks and Ottemöller (2001)], but that it missed on the dip angle by more than 40 degrees. Fig. 6 shows the intensities observed in the field for this earthquake (University of Bergen, 2003) after tessellation with Voronoi polygons (Pettenati *et al.*, 1999; Okabe *et al.*, 2000). Fig. 7 shows, by comparison, the pseudo-intensities produced by the minimum-variance model E2 in Table 3; note that several features of the experimental field in Fig. 6 are acceptably reproduced in Fig. 7.

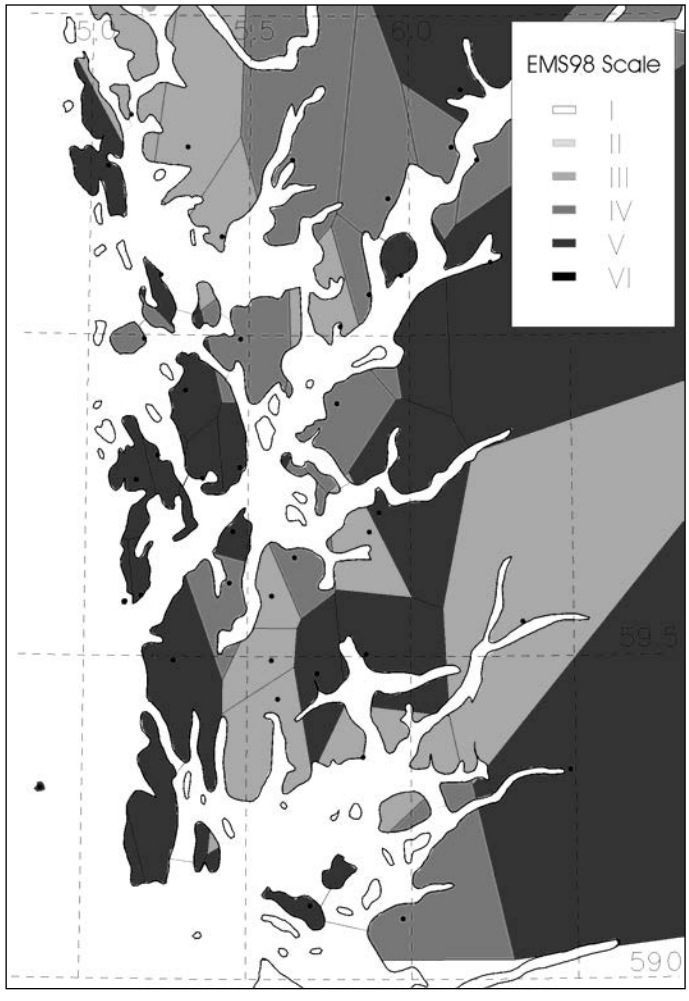

Fig. 6 - E2 earthquake of Dec. 08, 2000. Intensities observed at the sites by the University of Bergen (2003) tessellated by Voronoi polygons.

For event E3 (Fig. 5, lower right), the epicentral latitude and the strike and dip angles of the principal plane [as compared to the catalogue from the University of Bergen (2004)] are also well matched, as well as the basic dip-slip mode of faulting (see Section 2 for the ±180° ambiguity in the inverted rake angle). However, the inversion points to an almost pure dip-slip fault, possibly normal (260°±14°) while the rake angle

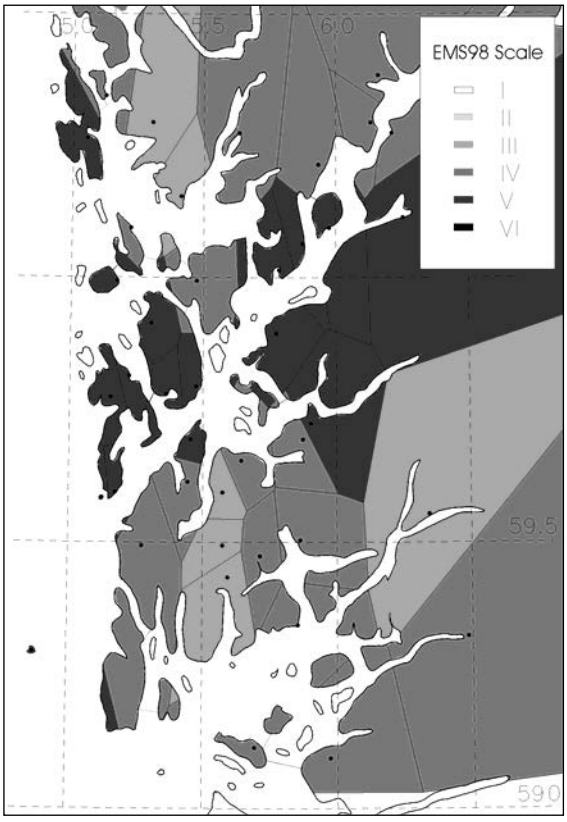

Fig. 7 - E2 earthquake of Dec. 08, 2000. Intensities calculated at the sites by using the best inversion solution of E2 shown in Table 3.

obtained from instrumental measurements is 305° (see Table 1), still normal, but with a significant (35°) horizontal component.

Finally, for event E4 (Fig. 5, upper right), we note that the NGA inversion was able to catch the focal mechanism quite well, as seen from a comparison between Tables 1 and 3.

As an additional test, we also calculated the minimum rotation of the P and T axes needed to overlap the inverted and the instrumental fault-plane solutions. Intuitively, small angles would validate the inversions, but no quantitative criteria are available to reject relatively high angles. We calculated these minimum rotations using the Kagan (1991) approach, and solved the +/-180° rake ambiguity in our technique by giving credit to the reference rake angles of Table 1. The results were: event E1: 71.4°; E2: 52.8°; E3: 64.4°; E4: 20.2°. In the case of the intensity inversion of the Whittier Narrows, 1987 earthquake (Gentile *et al.*, 2004), which we consider a well constrained and quite successful case, the minimum rotation was 29.7°.

With respect to the inverted seismic moment, we conclude that all of the inversion results are quite close to the instrumental values. However, from Tables 1 and 3 one can see that the inversions of the longitudes of the epicentres of events are often not well constrained, which is to be expected due to the partial lack of data towards the west, where the North Sea limits the observations.

The focal depths are omitted in Table 3 since our estimates are failing in this case, with values almost double the values given in Table 1. We believe that this is due to the use of a half-space in the *KF* model, and possibly also due to the fact that the transformation relation (4) refers back to earthquakes in the Los Angeles area (Sirovich and Pettenati, 1999).

4.3. A new i/KF empirical correlation for the Fennoscandian Shield – Caledonian Range transition area

Given that we have now inverted the intensity fields for the four events, this, in turn, provides a means for developing a new and updated relation between the kinematic *KF* functions and the site intensities *I*. To this end, we used the non-dimensional *KF* values, calculated at all the sites of the four earthquakes (from the sources of Table 3, but with the depths from Table 1), and the site intensities *I* observed in the field, resulting in Eq. (6). This new empirical relation was used to convert the *KF* site values into pseudo-intensity *i* for this part of the Fennoscandian Shield. Since Kvamme *et al.* (1995) demonstrated that body waves in this region prevail even beyond a distance of 150 km (i.e., the change from spherical to cylindrical spreading), we used 287 data from the whole 0-150 km range to calculate the following relation, after omitting the eight outliers of Table 2:

$$i(x,y) = 12.505\,(\pm 1.551) + 6.604\,(\pm 1.187)\cdot m[\log_{10} KF(x,y)] + 2.319\,(\pm 0.600)\cdot 10^{-17}\cdot M_0 \qquad (6)$$

$$R^2 = 0.77,$$

where *i(x,y)* is the pseudo-intensity to be forecasted at the site, at location (*x,y*) for earthquakes E1-E4, and M_0 is the seismic moment of E1-E4 in N · m. Pseudo-intensity *i* is truncated to an integer number.

Fig. 8 shows how Eq. (6) works with the data of the four earthquakes used to calculate the fitting function (see the thick lines in the figure). Note that in the figure the median values of log

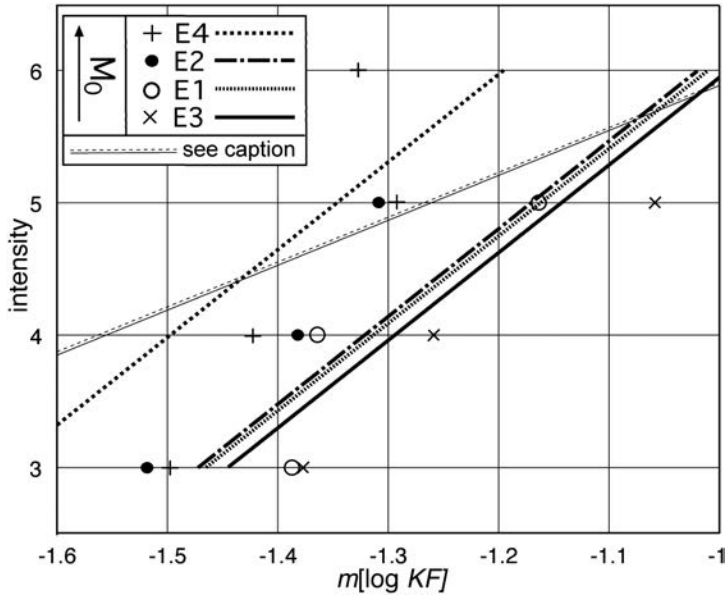

Fig. 8 - The thick lines refer to Eq. (6); the thin ones (extrapolated) to Eq. (4). Both Eqs. (4) and (6) fit the data of the four earthquakes used so that the regression lines are in the order of the magnitudes of the shocks, from that of E4 (M_w 5.2; see Table 1) to that of the smallest one (E3, M_L=4.0; see Table 1).

$KF(i)$ for event E4 (M_w=5.2, M_0=6.0 · 10^{16} N · m) are clearly separated from those radiated by the smallest one, E3 (M_0=2.1· 10^{15} N · m), with the data of the intermediate earthquakes in between (see Table 1). This behaviour basically confirms the behaviour of the Californian earthquakes that we used to develop our technique [Fig. 1 in Sirovich *et al.* (2001)]. The anomalous value of $m[\log_{10}KF]$ = -1.33 for I=6 of earthquake E4 in Fig. 8 is most likely caused by the absence of KF values close to the epicentre, which is far offshore (see Fig. 5); in turn, this made the R^2 value of Eq. (6) rather low (0.77). Eq. (6) can naturally be used only within the calibration ranges $2.1 \cdot 10^{15} \leq M_0 \leq 6.0 \cdot 10^{16}$ N · m, III ≤ I ≤ VI, and -2.402 ≤ logKF ≤ -0.436.

For comparison, Fig. 8 also shows the extrapolation of Eq. (4) in the range of the study earthquakes E1-E4. The different slopes of Eqs. (4) and (6) in Fig. 8 are due the different attenuations of intensity in California and in the Norwegian study area. Note that, at the M_0 level of earthquakes E1-E4, the four extrapolated logKF/I relations almost coincide; thus, to perceive the difference, Fig. 8 only shows the relation of the largest earthquake (E4, thin dashed line) and that of the smallest one (E3, thin continuous line).

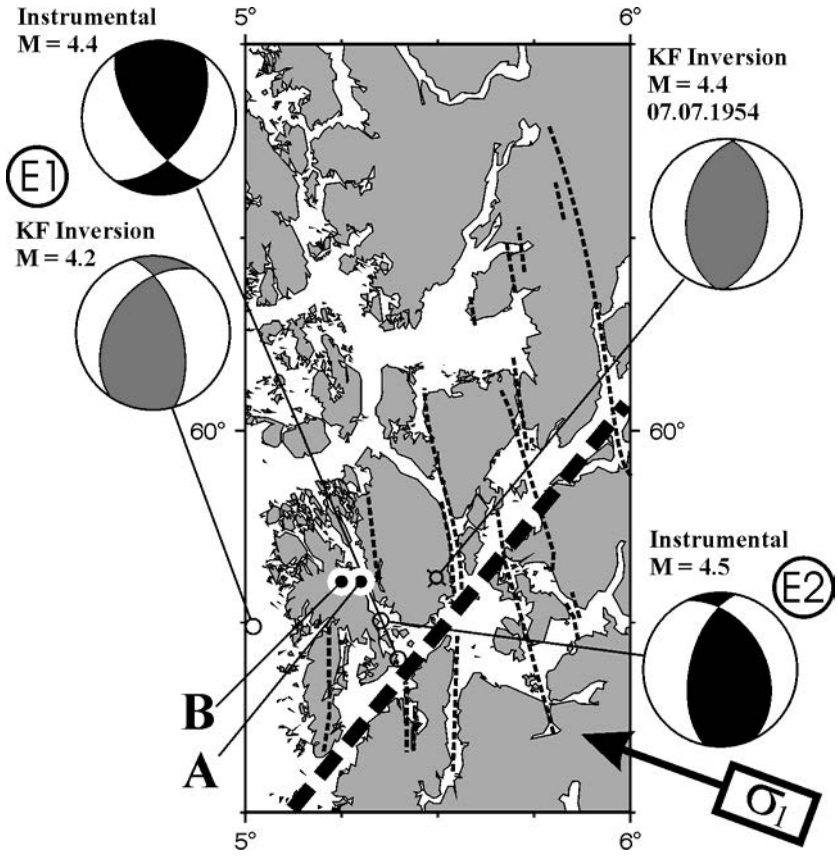

Fig. 9 - Close-up of the area of Figs. 1 and 2. The Hardanger Fjorden Shear Zone, trending SW-NE; the N-S and NNW-SSE trending faults; the fault-plane solution of the 1954 earthquake retrieved from the present intensity inversion; the fault-plane solution of E1 (both from P-wave polarities and from inversion); the instrumental fault-plane solution of E2 (see the text); σ_1 shows the orientation of the principal geodynamic horizontal compressive stress.

4.4. The ML 4.5 earthquake of July 7, 1954

After developing a new *KF* calibration for western Norway in Eq. (6), based on the four events, we used this in a new inversion of an M_L 4.5 earthquake of July 7, 1954, which also took place in the Stord region. The macroseismic data treated are by Muir Wood *et al.* (1988), using the MMI scale.

Let us recall here that Sellevoll (1957) used sparse instrumental data of the 1950s and placed the epicentre of this earthquake far offshore, 25 km west of that of E1. Then, Havskov and Bungum (1987) relocated this event somewhat northwest of the 1983 event (see Table 1; column A of Table 4, and Fig. 9). For this study, we were able to include additional seismogram readings published by the Bureau Central International de Séismologie (1954) and relocate the event by inverting all data with HYPOSAT (Schweitzer, 2001). This solution moved the epicentre a few kilometres eastward (Table 4, column B) and placed the hypocentre in the lower crust. As can be seen from columns A and B of Table 4, the depth of this earthquake is quite uncertain but the solution presented here places the event in the lower crust. The depth inverted from the observed intensities is close to the instrumental solution; whereas the new epicentre from the present study is approximately 13 km further to the east (see Table 4 and Fig. 9).

As already noted, the determination of the fault-plane solution using our inversion method is an almost bimodal problem for rake angles close to 90º and 270º (Pettenati and Sirovich, 2003). This is also the case for the 1954 event, because our NGA inversion points to an almost pure dip-slip mechanism, N-S-oriented. Thus, our solution contains the ambiguity between the principal and the auxiliary planes (see Table 4, columns P1 and P2, and Fig. 9); the intrinsic 180° ambiguity in the rake angle has also to be remembered. However, the mechanism found resembles those of events E1 and E2, and all three could tentatively correlate with N-S and NNW-SSE trending tectonic structures in the zone. The N-S and NNW-SSE trending faults in Fig. 9 are taken from Havskov and Bungum (1987). The three mechanisms shown in Fig. 9 are, therefore,

Table 4. The July 7, 1954 Stord earthquake, reference source parameters, independent from the present study.

Parametres	**A)**	**B)**	**P1)**	**P2)**
Latitude [°] N	59.80	59.80±0.05	59.81±0.08	59.81±0.08
Longitude [°] E	5.30	5.25±0.13	5.48±0.23	5.50±0.23
strike [°]			188±8	11±8
rake [°]			94±6	96±6
dip [°]			46±4	45±4
depth [km]	15	32±9	34.9±1.85	35±1.85
M_0 [N m]·10^{15}	9.54		6.2±1.95	6.2±1.95
mach +			0.97±0.015	0.96±0.015
mach -			0.95±0.012	0.94±0.012
Vs [km sec^{-1}]			3.63±0.07	3.63±0.07
Length [km] L+ = / L- =			L_{tot} = 1.6 0.40 / 1.20	L_{tot} =1.6 0.45 / 1.15

A): Havskov and Bungum (1987); also see Fig. 9
B): instrumental location, this study; the 9 km error of the depth corresponds to two standard deviations; also see Fig. 9
P1), P2): inversions from macroseismic data.

fully compatible with the orientation of the principal horizontal compressive stress σ_1 known also from earlier and more regional studies [Bungum *et al.* (1991) and Figs. 6d and 8d in Hicks *et al.* (2000a)].

5. Discussion and conclusions

In general, the starting point for this study was a difficult one in that we clearly aimed at exploring the limits for the intensity inversion method both in terms of the proximity to the sea and in terms of the low magnitudes employed.

The most difficult case was event E2 since only 41 intensity observations were available in that case (see Table 1). So, we made some tests to check the stability of the results obtained for this event. We repeated the inversion by using 10 sub-populations, and found 2923 solutions with exactly the same fitness $\sum r_s^2$=18 (our best inversion scored $\sum r_s^2$=17 in Table 3). These solutions have the same, or almost the same, hypocentral coordinates and fault-plane solution as for E2 in Table 3, but with some variations for the rest of the parametres. For example, the *Vs* values for the 2923 solutions span from 3.56 to 3.66 km/s (figure not shown here). Similar fluctuations are found for the Mach number, for *H*, *L*, and also for M_0. Thus, we conclude that in this case these parametres are less stable than the six parametres mentioned before.

We also prepared 10 data sets for E2 by removing 10% of the 41 observations with a Monte Carlo technique. Then, we inverted the remaining 37 data and found that seven out of ten solutions were identical to the one shown in Table 3, while three were considerably different. We then did the same by deleting 20% of the observations. In this case, only two out of ten solutions were similarly close to the best one in Table 3. From these tests, we conclude that our inversion is acceptably stable even for the event with the weakest data coverage.

Regarding E1, we feel more confident about our partial success because, in our experience with focal mechanism inversions, there is often more stability in terms of P and T axes than in terms of the fault planes, and this holds in the study case (and the orientation is compatible with the tectonic interpretations). We have already discussed the complex situation of the field data for event E2, and noticed that several features of the experimental field pattern are acceptably reproduced by the best synthetics in Fig. 7, inferred from the NGA inversion. But we also stressed that the price for this was the unsatisfactory simulation of the dip angle in the fault-plane solution. However, one more symptom of the effectiveness of the model behind Eq. (3) to simulate regional intensity patterns comes from Fig. 10, where the left part shows the synthetic *KF* field (dimensionless values) radiated by the Hicks and Ottemöller (2001) solution (see Table 1). Note, in particular, the two lobes radiated inland towards NE and SE. The right side of Fig. 10 shows the limit between the felt and the not-felt regions (labelled "F") obtained from the University of Bergen (2003) data. Regarding this, consider that in the catalogue used "not felt" is a significant piece of information because it means "reported not felt" (Jens Havskov, private communication). We stress that the "F" limit curve shown honours the experimental data strictly, without any smoothing or filtering effect, because we used the natural-neighbour interpolation [see Sirovich *et al.* (2002) about this contouring algorithm]. It is clearly not straightforward to make a quantitative comparison between the lobes on the left side of Fig. 10 and the "F" shape on the right side, but it seems that there is a tendency in both cases to elongate towards NE and SE, and

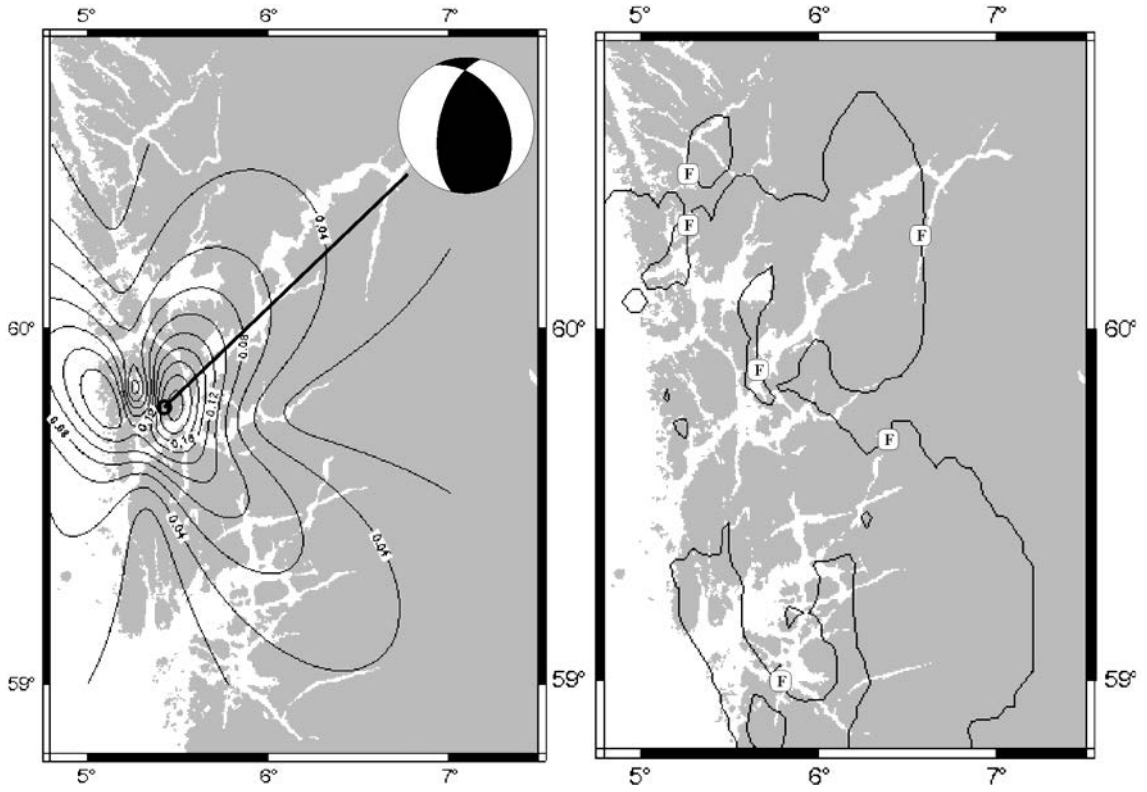

Fig. 10 - Left: The synthetic dimensionless *KF* field radiated by the source E2 obtainable from the reference data by Hicks and Ottemöller (2001) (see Table 1). Right: the felt/not-felt limit of E2 (field data of the Catalogue of the University of Bergen, 2003). The limit was obtained by the natural-neighbour interpolation (see the text).

to show a minimum towards east. In other words, the "F" limits seem to reflect the character of the source [for this, also see: Frankel (1994)].

The successful inversion of event E4 is also worth commenting; its instrumental epicentre is north of the others, where the coast bends, and is a lot more offshore (see Fig. 5), thus, more than half of the intensity field is missing. Notwithstanding this unfavourable situation, the NGA inversion was able to catch the reference source by Hansen *et al.* (1989) quite well (compare Tables 1 and 3). While this could seem surprising, some synthetic tests have confirmed that, in some cases, it is possible to delete an area of approximately 60% of the total intensity field without loosing the possibility of retrieving the source from the remaining part of the data. To some extent this holds even after perturbing the rest of the intensity pattern by substituting 7, 14, 21, and 28 percent of the remaining intensities by a Monte Carlo technique. In particular, we find that the most stable inverted source parametres are the five that determine the fault-plane solution and the epicentre location. Whereas, the along-strike and antistrike source lengths and rupture velocities are highly unstable (Sirovich *et al.*, 2004).

From a comparison between Tables 1 and 3, and from Fig. 5, it is clear that our inversions were able to match the reference source parametres well only in some cases. On this crucial point, we note as follows.

• The fault-plane solutions and the instrumental epicentres are obtained from the first, low-

amplitude, recorded pulses, that come from early subruptures, and are carried by relatively high frequencies. On the other hand, the regional intensity pattern is caused by the whole rupture and by relatively low frequencies. Thus, in general, for large earthquakes, we are speaking about two different things, and a perfect match between them is difficult. But, in the cases studied, the events are so small that only minor discrepancies are expected.

- The Norwegian earthquakes studied here were smaller in magnitude than those we had previously used to formulate our algorithm and to perform the validation tests, which reflects on the comparison between the Californian and the Norwegian *i/KF* empirical correlations in Fig. 8.
- Notwithstanding the limited accuracy of our present results, they are still interesting since they imply an extended and more complete exploitation of pre-instrumental data. Given the long return times for the largest earthquakes in the region, such improvements are valuable.

Therefore, in spite of some significant deviations between instrumental and inversion results, the match is still generally good, vouching positively for the possibilities to use this method on pre-instrumental earthquakes for which only little and uncertain information is usually available. One such event is the M_L 4.5 earthquake of July 7, 1954, where an instrumental solution is not within reach. While this solution cannot therefore be validated, it is supported by the validation of later events from the same region. Moreover, the results obtained are tectonically and geodynamically plausible.

In conclusion, the present work was a hard but still a reasonably successful test for our technique. In fact, we treated low-magnitude earthquakes under non-ideal test conditions, because of the asymmetric distribution of the sites surveyed in the field close to the ocean coast. In spite of this, we found that the inversions were acceptably validated by independent information in three of the four cases tested. Thus, also in such cases it may be possible to get an approximate idea of the source of an earthquake by inverting its regional intensity pattern. This encourages us to go ahead and use this method for more earthquakes from the pre-instrumental era.

Acknowledgments. This research was supported by a grant from Istituto Nazionale di Geofisica e Vulcanologia (INGV) in Rome, and one of us (FP) was also supported by a fellowship to NORSAR under the European Commission's Programme Improving Human Research Potentials, Transnational Access to Research Infrastructure (Contract HPRI-CT-2002-00189). We thank Jens Havskov for generously providing us with macroseismic data and fault-plane solutions for the Norwegian earthquakes studied. We very much appreciate the detailed and constructive comments of the referees Dario Albarello and Paolo Gasperini, which significantly improved the quality of the paper. One suggestion by the latter reviewer, about rotation of double couples, has also given us valuable ideas for future work.

REFERENCES

Aki K. and Richards P.G.;1980: *Quantitative Seismology*. Theory and Methods, W.H. Freeman & Co, San Francisco, 932 pp.

Azzaro R. M., Barbano S., Moroni A., Mucciarelli M. and Stucchi M.; 1999: *The seismic history of Catania*. J. of Seismology, **3**, 235-252.

Bakun W. H. and Wentworth C. M.; 1997: *Estimating earthquake location and magnitude from seismic intensity data.* Bull. Seism. Soc. Am., **87,** 1502-1521.

Barnett V. and Lewis T.; 1978: *Outliers in statistical data*. Wiley series in probability and mathematical statistics-applied, John Wiley and Sons, Chichester, 355 pp.

Bernard P. and Madariaga R.; 1984: *A new asymptotic method for modeling of near-field accelerograms*. Bull. Seism. Soc. Am., **74**, 539-557.

Bungum H., Alsaker A., Kvamme L.B. and Hansen R.A.; 1991: *Seismicity and seismotectonics of Norway and surrounding continental shelf areas*. J. Geophys. Res., **96**, 2249-2265.

Bungum H., Lindholm C. and Faleide J. I.; 2004: *Postglacial seismicity offshore mid-Norway with emphasis on spatio-temporal-magnitudal variations*. Marine and Petroleum Geology, **22**, 137-148.

Bungum H., Pettenati F., Sirovich L. and Schweitzer J.; 2004: *Source inversion of regional intensity patterns: the Ms=5.5, 1904 Oslofjord earthquake, and some smaller well-recorded Norwegian events*. In: E.S.C. XXIX Gen. Ass. Abstracts, University and GFZ, Potsdam, pp. 98.

Bureau Central International de Séismologie; 1954: Julliet 1954. Strasbourg.

Byrkjeland U., Bungum H. and Eldholm O.; 2000: *Seismotectonics of the Norwegian continental margin*. J. Geophys. Res., **105**, 6221-6236.

Camassi R. and Stucchi M.; 1997: *NT4.1.1 Un catalogo parametrico di terremoti di area italiana al di sopra della soglia del danno*. http://emidius.mi.ingv.it/NT/home.html.

Frankel A.; 1994: *Implications of felt area-magnitude relations for earthquake scaling and the average frequency of perceptible ground motion*. Bull. Seism. Soc. Am., **84,** 462-465.

Gentile F., Pettenati F. and Sirovich L.; 2004: *Validation of the automatic nonlinear source inversion of the U. S. Geological Survey intensities of the Whittier Narrows, 1987 earthquake*. Bull. Seism. Soc. Am., **94**, 1737-1747.

Hanks T.C. and Kanamori H.; 1979: *A moment magnitude scale.* Journal of Geophysical Research, **84**, 2348-2350.

Hansen R.A., Bungum H. and Alsaker A.; 1989: *Three recent larger earthquakes offshore Norway*. Terra Nova, **1**, 284-295.

Havskov J. and Bungum H.; 1987: *Source parametres for earthquakes in the northern North Sea*. Nor. J. of Geol., **67**, 51-58.

Hicks E., Bungum H. and Lindholm C.; 2000a: *Stress inversions of earthquake focal mechanism solutions from onshore and offshore Norway*. Nor. J. of Geol., **80**, 235-250.

Hicks E.C., Bungum H. and Lindholm C.D.; 2000b: *Seismic activity, inferred crustal stresses and seismotectonics in the Rana region, northern Norway*. In: Stewart I.S., Sauber J. and Rose J. (eds), Glacio-seismotectonics: Ice Sheets, Crustal Deformation and Seismicity, Quaternary Science Reviews, **19**, 1423-1436.

Hicks E. and Ottemöller L.; 2001: *The ML 4.5 Stord/Bømlo, southwestern Norway, earthquake of 12 August 2000. Nor*. J. of Geol., **81**, 293-304.

Johnston A.C.; 1996a: *Seismic moment assessment of earthquakes in stable continental regions - I. Historical seismicity*. Geophys. J. Int., **124,** 381-414.

Johnston A.C.; 1996b: *Seismic moment assessment of earthquakes in stable continental regions - II. Historical seismicity*. Geophys. J. Int., **125,** 639-678.

Kagan Y.Y.; 1991: *3-D rotation of double-couple earthquake sources*. Geophys. J. Int., **106**, 709-716.

Kawase H. and Aki K.; 1990; *Topography effect at the critical SV-wave incidence: possible explanation of damage pattern by the Whittier Narrows, California, earthquake of 1 October 1987*. Bull. Seism. Soc. Am., **80**, 1-22.

Kennett B. L. N. and Sambridge M. S.; 1992: *Earthquake location - genetic algorithms for teleseisms*. Phys. Earth Planet. Interiors, **75**, 103-110.

Koper K. D. L., Wysession M. E. and Wiens D. A.; 1999: *Multimodal function optimization with a niching genetic algorithm*, Bull. Seism. Soc. Am., **89**, 978-988.

Kvamme L.B., Hansen R.A. and Bungum H.; 1995: *Seismic source and wave propagation effects of Lg waves in Scandinavia.* Geophys. J. Int., **120**, 525-536.

Levine D.; 1996. *Users guide to the PGAPack parallel genetic algorithm library,* Report Argonne National Laboratory ANL-95/18, Argonne, IL, 73 pp.

Madariaga R. and Bernard P.; 1985: *Ray theoretical strong motion synthesis*. J. Geophys, **58,** 73-81.

Martin L. S, Scales J. A. and Fischer T. L.; 1992: *Global search and genetic algorithms*. The Lead. Edge, **2,** 22-26.

Moya A., Aguirre J. and Irikura K.; 2000: *Inversion of source parameters and site effects from strong ground motion records using genetic algorithms*. Bull. Seism. Soc. Am., **90**, 977-992.

Møllegaard E.; 2000: *Seismotectonics in the northern North Sea*. Cand. Scient. thesis, University of Oslo, 142 pp., in Norwegian.

Molchan G.M., Kronrod T.L. and Panza G.F.; 2004: *Shape of empirical and synthetic isoseismals: comparison for Italian M≤6 earthquakes*. Pure Appl. Geophys., **161**, 1-23.

Muir Wood R., Woo G. and Bungum H.; 1988: *The history of earthquakes in the northern North Sea*. In: Lee W.H.K., Meyers H. and Shimazaki K. (eds), Historical Seismograms and Earthquakes of the World, Academic Press, San Diego, pp. 297-306.

Okabe A., Boots B., Sugihara K. and Chiu S. N.; 2000: *Spatial tessellation*. Wiley, Chichester, (2nd ed.) 671 pp.

Pettenati F., Sirovich L. and Cavallini F.; 1999: *Objective treatment and synthesis of macroseismic intensity data sets using tessellation*. Bull. Seism. Soc. Am., **89**, 1203-1213.

Pettenati F. and Sirovich L.; 2003: *Tests of source-parameter inversion of the U.S. Geological Survey intensities of the Whittier Narrows 1987 earthquake*. Bull. Seism. Soc. Am., **93**, 47-60.

Press W.H, Teukolsky S.A., Vetterling W.T. and Flannery B.P.; 1992: *Numerical recipes in Fortran; the art of scientific computing*. Cambridge University Press (second ed.), Cambridge, 963 pp.

Schweitzer J.; 2001: *HYPOSAT – An enhanved routine to locate seismic events*. Pure and Applied Geophysics, **158**, 277-289.

Sellevoll M. A.; 1957: *Earthquake in the Norwegian Channel on the 7th and 10th of July 1954*. Universitetet i Bergen, Årok, Mat. Nat. ser.2, 1-28.

Shebalin N. V.; 1973: *Macroseismic data as information on source parameters of large earthquakes, Phys*. Earth Planet. Interiors, **6**, 316-323.

Shebalin N. V.; 2003: *Quantitative macroseismic*. In: Keilis-Borok V.I. and Molchan G.M. (eds), Collection of Scientific Proceedings in Computational Seismology, Moscow, pp. 57-200, in Russian.

Sirovich L.; 1982: *Emergency microzonations by Italian Geodynamics Project after November 23, 1980 earthquake: a short technical report*. In: Proc. 3rd Int. Conf. on Microzonation, Seattle USA, pp. 1417-1427.

Sirovich L.; 1996: *A simple algorithm for tracing out synthetic isoseismal*s. Bull. Seism. Soc. Am., **86,** 1019-1027.

Sirovich L.; 1997: *Synthetic isoseismals of three earthquakes in California-Nevada*. Soil Dyn. and Earthq. Eng., **16**, 353-362.

Sirovich L. and Pettenati F.; 1999: *Seismotectonic outline of South-Eastern Sicily: an evaluation of available options for the scenario earthquake fault rupture*. J. of Seismology, **3**, 213-233.

Sirovich L. and Pettenati F.; 2001: *Test of source-parameter inversion of the intensities of a 54,000-death shock of the XVII Century in SE Sicily*. Bull. Seism. Soc. Am., **91**, 792-811.

Sirovich L. and Pettenati F.; 2004: *Source inversion of intensity patterns of earthquakes; a destructive shock in 1936 in NE Italy*. J. Geophys. Res., **109**, 109, B10309, doi:10.1029/2003LB0029919, 16 pp.

Sirovich L., Pettenati F. and Chiaruttini C.; 2001: *Test of source-parameter inversion of intensity data*. Natural Hazards, **24**, 105-131.

Sirovich L., Pettenati F., Cavallini F. and Bobbio M.; 2002: *Natural-Neighbour isoseismals*. Bull. Seism. Soc. Am., **92**, 1933-1940.

Sirovich L., Bobbio M., Gentile F. and Pettenati F.; 2004: *SITAR – Engineering Seismology Group*. In: OGS, Oceanography Department Annual Report 2003, OGS, Trieste, pp. 67-71, PDF file in: http://www.ogs.trieste.it/OGS/oga/home_oga.htm

Spudich P. and Frazer L. N.; 1984: *Use of ray theory to calculate high-frequency radiation from earthquake sources having spatially variable rupture velocity and stress drop*. Bull. Seism. Soc. Am., **74**, 2061-2082.

University of Bergen; 2003: *Seismological Bulletin from Norwegian National Seismic Network,* Seismological Observatory, Dept. of Earth Sciences.

University of Bergen; 2004: *Bergen Monthly Bulletins from the Norwegian National Seismic Network,* Seismological Observatory, Dept. of Earth Sciences.

Wells D. L. and Coppersmith K. J.; 1994: *New empirical relationships among magnitude, rupture length, rupture width, rupture area, and surface displacement*. Bull. Seism. Soc. Am., **84**, 974-1002.

Corresponding author: Franco Pettenati
Istituto Nazionale di Oceanografia e di Geofisica Sperimentale - OGS
Borgo Grotta Gigante 42/c, Sgonico (Trieste), Italy
phone: +39 0402140317; fax: +39 040327307; e-mail: fpettenati@ogs.trieste.it